PHYSICAL REVIEW E **89**, 013011 (2014)

Unorthodox bubbles when boiling in cold water

Scott Parker[1] and Steve Granick[1,2]

[1]*Department of Materials Science and Engineering, University of Illinois, Urbana, Illinois 61801, USA*

[2]*Department of Chemistry and Department of Physics, University of Illinois, Urbana, Illinois 61801, USA*

(Received 26 September 2013; revised manuscript received 3 December 2013; published 15 January 2014)

High-speed movies are taken when bubbles grow at gold surfaces heated spotwise with a near-infrared laser beam heating water below the boiling point (60–70 °C) with heating powers spanning the range from very low to so high that water fails to rewet the surface after bubbles detach. Roughly half the bubbles are conventional: They grow symmetrically through evaporation until buoyancy lifts them away. Others have unorthodox shapes and appear to contribute disproportionately to heat transfer efficiency: mushroom cloud shapes, violently explosive bubbles, and cavitation events, probably stimulated by a combination of superheating, convection, turbulence, and surface dewetting during the initial bubble growth. Moreover, bubbles often follow one another in complex sequences, often beginning with an unorthodox bubble that stirs the water, followed by several conventional bubbles. This large dataset is analyzed and discussed with emphasis on how explosive phenomena such as cavitation induce discrepancies from classical expectations about boiling.

DOI: 10.1103/PhysRevE.89.013011 PACS number(s): 47.55.dd, 64.60.Q−, 47.80.Jk, 47.55.pb

I. INTRODUCTION

Not enough is understood about boiling. So familiar in one's daily life that it can be taken for granted, it also presents a fundamental problem of nonequilibrium physics and on the practical side, it is of mounting importance to technologies such as development of high heat-flux surfaces needed for safe and reliable performance of nuclear reactors and microchip systems. Engineers have a long tradition of appreciating the potential to use boiling to practical ends, and in the engineering literature, studies have investigated effects of surface morphology [1–6], surface chemistry [4,7–10], and even the angle of inclination [10–13] of the boiling surface on how well hot surfaces transfer heat. Many of these studies have often been accompanied by numerical models of the heat transferred by a single vapor bubble [3,5,14–17] and have been scaled up to predict macroscopic behavior. Inevitably, model-dependent simulations assume a certain bubble geometry and interaction with a surface, however.

Here we describe high-speed optical imaging of individual bubbles as they form and detach, one by one. Relative to prior work, the new point is the following. In one approach, prior experiments heated a large area of solid surface and studied the cooling produced by boiling [4,14,18–21] but while important, such studies show only by inference the life cycles of individual bubbles, thus limiting their predictive power at the microscale. In the alternative approach of studying single bubbles, pulsed lasers and lithographically patterned microheaters were used to generate uniform single bubbles [22–28]. But in this approach, even if the average power is low, the peak local power can be high, and while this situation is quite relevant to ink-jet printing [24,20], it is not representative of many other practical applications. The work reported here considers the middle ground: We study individual bubbles by heating the substrate spotwise with continuous application of heating power. Part of the motivation to take this approach is that regarding applications, it might be representative of the heating produced by hundreds of transistors continuously switching on a microchip cooled by surrounding water.

In the study presented below, image analysis of high-speed movies has been used extensively and a large dataset has been analyzed statistically. We conclude that while the naive scenario of boiling is observed under some conditions, patterns of boiling decidedly more complex also contribute significantly. The naive scenario is considered to be this: that in a superheated liquid region adjacent to the heated solid, bubbles grow on a nucleation site and upon exceeding a critical size, buoyancy overcomes surface tension force pinning the bubble to the surface and the bubble pinches off, allowing cooler surrounding liquid to flow in. Tentative explanations are proposed of when to expect deviations from this.

II. EXPERIMENTAL SECTION

A closed cell was mounted onto the homebuilt microscope as depicted in Fig. 1(a) and filled with deionized water. In the optical path used for heating, a cw laser (OptoEngine, $\lambda = 800$ nm, power continuously variable up to 5 W) was focused onto the sample surface using a 20× long-working distance objective (Mitutoyo). Laser power was constant throughout the boiling experiment. A mechanical shutter with an opening time of 0.7 ms (Uniblitz LS6, not shown) was used to block the laser beam when not in use. The laser beam had a $1/e$ diameter of 314 μm as measured by a knife-edge technique. The surface temperature was measured by optical reflectivity. This information and the measured laser radius were used to estimate the steady-state temperature field generated by the laser heating in the surrounding water, with results summarized in Fig. SM1 of the Supplemental Material [49]. Briefly, these numerical simulations showed that heating a circular surface area produces a nearly hemispherical dome of heated liquid that extends to approximately the same height as the diameter of the heated surface, which was 300 μm for the parameters of this experiment.

The shape of resulting bubbles was recorded by bright-field microscopy in an optical path parallel to the heated surface. For this, illumination was provided by a pulsed light emitting diode (LED; Light Speed Technologies, 630 nm) mounted behind the sample, with pulses synchronized to image acquisition by a

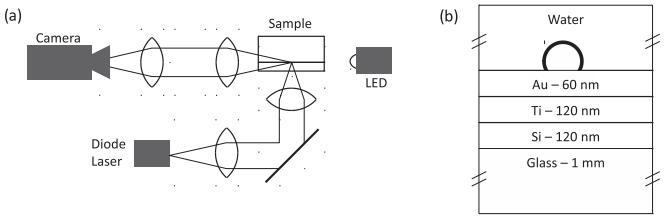

FIG. 1. Optical instrument setup. (a) The sample is heated by a high-power 800 nm diode laser which is focused onto the sample through a homebuilt microscope. In parallel, a high-speed video camera, illuminated by an LED, is used to visualize bubbles with a frame rate up to 50 000 fps and exposure time down to 10 ns. (b) The water sample cell and the boiling bubbles formed within it sit on a glass slide with the indicated multilayer coating: Si to measure near-surface temperature by optical reflectivity, Ti to absorb heat, and Au capping layer to avoid oxidation of Ti.

high-speed camera (Vision Research Phantom 7.3). Pulsing the LED allowed us to acquire high contrast images with insignificant heating of the sample by the illumination source. Images were recorded up to 50 000 frames per second.

The sample surface consisted of layers of sputtered metal films on a glass slide as depicted in Fig. 1(b), with the heating laser beam introduced through the glass onto the metal films. First, a 120 nm Si base layer, nearly transparent to the heating laser, was deposited for thermoreflectance measurements to measure surface temperature. Next, a 120 nm Ti layer was deposited, but as titanium oxidizes when exposed to air, this would be problematic as oxides of titanium have photoswitchable wettability [29–33]. In order to prevent oxidation the Ti was capped by a 60 nm Au layer. This was designed to be sufficiently thick that the power of the heating laser would be attenuated to a power level sufficiently low not to expect optical trapping of the growing vapor bubbles.

A complication was that the optical characteristics of these layered films were found to depend on precise thin-film deposition conditions that could not be controlled. To compensate for this, for each sample the reflectivity and transmission was measured in a UV-visible spectrophotometer (Sinco S-4100) at 800 nm. This information, combined with measurements of the incident laser power, allowed us to determine accurately the precise heating power applied in each experiment. Factoring in the known absorption and reflectivity of each sample, the actual heating power was up to 3 W with 86% of the power distributed over a circle with radius 314 μm.

The boiling chamber consisted of an aluminum block ($1'' \times 1.25'' \times 2.5''$) with a cavity ($0.5'' \times 1.25'' \times 1''$) in which boiling took place. Windows in the bottom and sides allowed us to view the sample during boiling. To clean the cell between successive experiments, heated deionized water (70 °C) was pumped (10 min) through the chamber to equilibrate the temperature and also flush out any bubbles left on the surface from the earlier experiment. The system was left to equilibrate

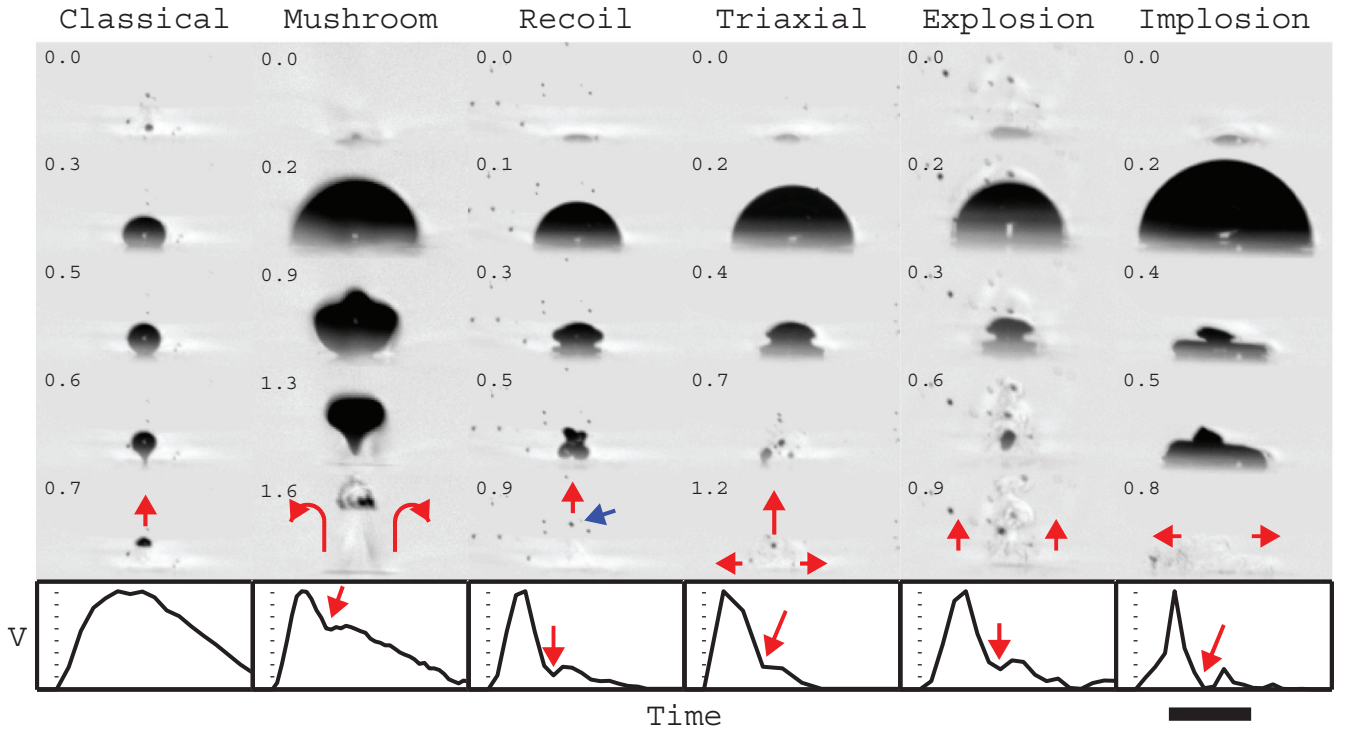

FIG. 2. (Color online) Each column illustrates a different bubble departure mode. Each successive row from the top shows how bubble shape changes with time. Time, counted in milliseconds since the bubble became large enough to see, is shown in numerals alongside each image. Arrows in the bottom row of images show the direction of flow by surrounding water, inferred from the direction in which the bubble moves. For the specific case of the recoil sequence, the darker blue arrow points to the departing bubble to distinguish it from nearby ambient bubbles [49]. On the bottom row, image analysis has been used to plot bubble volume against elapsed time for the bubble in that departure sequence. In each plot, the red arrow shows the time at which the collapse ratio (ratio of largest volume to volume after initial collapse) was evaluated. At the very bottom, the scale bar is 1 mm.

without pumping (1 min, over which the temperature in the sample fell to 66 °C). After these preparations, the sample was exposed to the heating laser for 2 s while images were acquired with the high-speed camera. This cycle was repeated an average of 50 times per sample. Images were of course distorted by thermal lensing, as can be easily identified in the top row of Fig. 2, but this did not detract from the bubble shape analysis presented below.

III. RESULTS AND DISCUSSION

The time evolution of approximately 5000 bubbles was imaged optically during their growth and detachment cycles, and was evaluated according to how they grew, how their sizes ultimately diminished, how they broke up into other bubbles, and the direction in which they migrated after breakup. When the heating power was just sufficient to produce boiling, bubbles grew and detached in repetitive succession. At the extreme of high heating power, bubbles often grow to a stable size without detaching. Between these extremes, we observed the broad spectrum of behavior summarized below.

A. Bubble types

Among the common features are these: First, bubble volume invariably diminished after bubbles detached from the heated solid, which is natural as the surrounding liquid was cooler. Second, the volume of many bubbles also diminished before detachment, at the point when these bubbles had grown large enough to be cooled by surrounding water. To refer to shrinking of height and width before detachment, we will use the term "bubble collapse." Third, instabilities were sometimes observed when bubbles collapsed rapidly, at speeds up to 4 m/s. Then, when the amplitude of instability became comparable to the size of these shrinking bubbles, the bubbles fragmented into smaller bubbles before detachment. This fragmentation of bubbles that have not yet detached from the heated surface, we will refer to as "breakup." Fourth, we followed the direction, relative to the surface, of bubbles when they departed. As tracer particles to visualize the flow field might have interfered with nucleation, to estimate the flow we simply followed the paths of departing bubbles.

Figure 2 presents a large tabulation of images describing the six bubble types we have identified, and Table I explains the detachment mode of each of them: These types are classical, mushroom, recoil, triaxial, explosion, and implosion. Among these, recoil and triaxial are closely related to mushroom and explosion modes, respectively, but warrant their own discussion. While of course there is a continuum of behavior, these six categories are a convenient and concise way in which to discuss them, much as we utilize discrete colors to describe a rainbow.

TABLE I. Criteria to define bubble type.

	Collapse	Breakup	Flow direction[a]
Classical			↑
Mushroom	×		↑
Recoil	×[b]		↑
Triaxial	×	×[c]	↑
Explosion	×	×	↑
Implosion	×	×	↓

[a]↑ denotes away from surface; ↓ denotes towards.
[b]Rayleigh-Taylor instabilities present.
[c]Breaks into three distinct parts.

1. *Classical bubbles*

Most common are the images in the first column of Fig. 2: "classical" bubbles. They grow uniformly in each direction while maintaining a nearly constant radius of curvature. As they pinch off the surface into colder surrounding water, a neck forms, the result of competition between buoyancy and surface tension at the contact line, but the bubble's top remains spherical. As the bubble rises into cooler water, the bubble shrinks and its shape becomes even closer to spherical. This is partly because vapor within the bubble condenses, partly because hydrodynamic flows encourage the rising bubbles to take a spherical cap shape [34]. Classical bubbles leave the surface vertically. Their departure is driven principally by buoyancy. Break up into smaller bubbles is not observed.

2. *Implosion bubbles*

Conceptually, these are the opposite of classical bubbles. Instead of gently lifting off the surface under the action of buoyancy, implosion bubbles first grow rapidly, then collapse, ultimately breaking up into many residual bubbles. In contrast to all other bubble modes, the rate of height reduction is faster than the rate of width reduction [Fig. 3(a)], even well before the destructive breakup of the bubble. Flow resulting from the collapse drives the residual bubbles away from the nucleation site, parallel to the surface as indicated in the last column of Fig. 2. From conservation of mass balance, it is then obvious that from the direction normal to the surface, water must be drawn towards the surface.

This collapse followed by parallel ejection of residual bubbles is analogous to what happens with cavitation bubbles and vapor explosions [35–40]. In such experiments, the common element is to create a bubble whose vapor pressure exceeds that of its immediate surroundings. These bubbles expand rapidly until growth is arrested by surface tension. Without sufficient damping, they expand beyond their equilibrium size, then collapse. It is known that when cavitation bubbles form close to a rigid wall, the symmetry loss presented by the wall causes a singular jet to penetrate the bubble and strike against the wall [39–44], but studies of this kind were not made in the context of boiling.

When cavitation is induced thermally, energy is injected in submicrosecond pulses so there is no time for heat to build up in the surrounding fluid. Therefore bubble motion is determined by inertial expansion of the bubble against the surrounding fluid. Once the bubble reaches its maximum size, as it contains no more mass than at its original size, this provides a strong driving force for collapse. But with boiling, heating of water is slower and steadier, and this allows water to evaporate along the edge of bubbles [45]. The mass of vapor contained within the bubble has time to increase and this discourages collapse of the bubble. This is observable in Fig. 2 when the bubble reached a local minimum in size at 0.4 μs. In the absence of

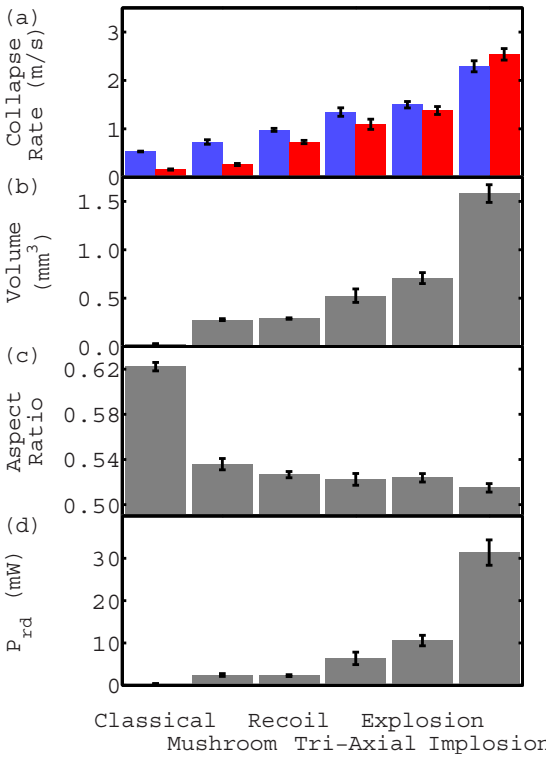

FIG. 3. (Color online) Size and shape parameters. (a) Collapse rate after reaching maximum volume, calculated alternatively from the bubble height dH/dt (left) and bubble width $(1/2)dW/dt$ (right). (b) Aspect ratio (H/W) at maximum volume; (c) maximum volume; (d) estimated kinetic energy imparted into the surrounding liquid during bubble growth.

evaporation it would have continued to collapse to a near-zero volume before rebounding, but collapse was arrested by the evaporated vapor. In spite of the presence of evaporation, and since bubbles form in such a different way from traditional cavitation, it is surprising to see the common phenomenology just described.

The fact that implosion bubbles nucleate at the heated solid, unlike typical cavitation bubbles, leads to other differences. Typically, the implosion bubbles that we observed did not become as large as normal cavitation bubbles would be expected to become if they were nucleated under otherwise similar conditions. This is probably because growth is impeded by an additional dissipation channel: When implosion bubbles wet the solid with a three-phase contact angle between solid, liquid, and vapor, this dissipates energy through the contact angle hysteresis of the surface and pinning [46–48]. In Fig. 2, the images of implosion-bubble collapse at 0.4 and 0.5 μs show this influence. Whereas true cavitation bubbles collapse uniformly in all directions, the presence of the nearby solid slows down the collapse of implosion bubbles, especially their lateral collapse. This causes large amplitude instabilities to form along the surface of the bubble, generating layers instead of a single penetrating jet from the top.

Of course another natural explanation for the shape of the collapsing bubble is that as implosion bubbles grow very rapidly, a thin boundary layer of water remains on the surface between the bulk phase of the bubble and the substrate [14,22]. Such a microlayer would lead to a high curvature along the apparent contact line at the edge of the bubble, and would introduce capillary waves along the bubble surface as the curvature relaxes. This may occur when the superheating is small. However, as the bubble shape evolves, we observe that bubbles remain adjacent to the surface instead of beginning to lift off, suggesting that the contact line is relatively immobile. Furthermore, high-speed thermoreflectance measurements of surface temperature below unorthodox-shaped bubbles have suggested that this microlayer has evaporated by the time the bubble begins to collapse [49,50].

3. *Explosion bubbles*

Other bubbles are observed to "explode." After they grow like implosion bubbles (nearly hemispherical shape during rapid growth, overexpanded radius, and finally collapse), they too broke up into many smaller bubbles. Explosions generated flow away from the surface as the bubbles departed.

A special case is the triaxial bubble. In this mode, bubbles fractionate into three distinct sub-bubbles as demonstrated in Fig. 2 in the image taken at 0.7 ms. The bubble's thermal instabilities caused a layered structure to form. With growing instability amplitude, the top layer pinched off and departed rapidly. The bottom of the bubble split into two sub-bubbles and began to spread along the surface but more slowly than the vertical bubble departed. Many such sub-bubbles spread in multiple different directions, in this particular case asymmetrically though with the principal flow direction away from the surface. Visually it looks like an explosion.

4. *Mushroom-shaped bubbles*

When collapse of bubbles is only partial, then buoyancy dominates, and the shape resembles the iconic mushroom cloud of a nuclear explosion. As the bubble starts to rise, its top flattens due to condensation driven by the surrounding cooler fluid. While capillary waves are certainly present and give rise to variations in the shape at 0.9 ms, the bubble height remains fixed during most of the bubble lifetime, confirming that condensation plays the dominant role in modifying the shape [49]. In the meantime, buoyancy continues to drive the bubble upward, leaving a thin neck stretching down to the nucleation site. In Fig. 2, an image (1.3 ms) illustrates this. Later as this bubble rose higher, its neck detached to form a reentrant jet that pierced the bubble's top surface. This formed a toroid which ultimately broke up into smaller bubbles. Because of the high velocity of the reentrant jet through the center of the bubble, rotational flow drew water inwards from the sides, up the center, and away from the heated surface, as illustrated in the final image of the sequence in Fig. 2. Thus, the mushroom bubble detached from the surface as a single bubble; later, it broke up into many bubbles, the result of flows generated away from the surface.

A related case is the recoil bubble. Resembling mushroom bubbles, they break up only after detaching from the surface. The difference is that along their surfaces they display substantial instability as the bubble collapses, much as explosion and triaxial bubbles do. As illustrated in Fig. 2 by the image taken at 0.5 ms, compression of the vapor within the bubble

caused the bubble to reexpand before it broke up. Buoyancy then lifted this bubble off the surface.

B. Size and shape parameters

We now consider quantification, beyond the qualitative trends just summarized.

1. Collapse ratio

The slow growth of bubbles by evaporation along the bubble surface (growth until buoyancy of the growing bubble overcomes surface pinning forces) can be more complex than the classical picture of boiling because in the absence of strong viscous damping, bubbles can exhibit a rapid overexpansion of volume, driven by a high initial vapor pressure which exceeds the surrounding pressure. These same bubbles then rapidly collapse to a volume closer to the equilibrium value. The ratio, maximum volume to volume after the initial collapse, is denoted by the red arrow in the volume plots of Fig. 2. This we refer to as the "collapse ratio."

There is a tendency for the collapse ratio to increase in the sequence of columns in Fig. 2, from classical to implosion bubbles, indicating that a progressively greater portion of the growth is driven by inertial expansion rather than evaporative growth. For example, implosion bubbles exhibit complete collapse but classical bubbles do not collapse at all (although they do shrink as they rise into the colder surrounding fluid).

2. Lifetime

In the sequence of classical, mushroom, recoil, triaxial, explosion, and implosion bubbles, there is progressive increase in the average maximum volume of the bubble [Fig. 3(b)]. Each growth mode represents an average volume, with implosion bubbles having the largest average volume.

Size did not correlate with lifetime. The majority of bubbles had a lifetime of 0.7 ms regardless of their growth mode (Fig. SM7, Supplemental Material [49]). This implies that the larger the bubble volume, the faster the bubble collapse rate must be. However, the vertical and lateral collapse rates can differ. For the most rapidly collapsing bubbles their vertical collapse rate was faster than their lateral collapse rate, whereas for all other bubbles, the lateral collapse rate was faster. Classical bubbles display no vertical collapse at all as the sole collapse mechanism is condensation into the surrounding liquid [Fig. 3(a)].

The more rapid vertical collapse rate is even more spectacular when one considers that as the bubble size and collapse rate increases, the aspect ratio decreases, until at their maximum size they are nearly hemispherical [Fig. 3(c)]. Furthermore, not only does aspect ratio decrease from classical to implosion bubbles, but so does the variability (Fig. SM7, Supplemental Material [49]). Hemispherical growth is further evidence of the inertial growth of the vapor bubble [35,51,52]. Parenthetically, we note that care should be taken in interpreting aspect ratio for classical bubbles in Fig. 3(c). Comparison with Fig. 2 shows that classical bubbles are still quite spherical and exist as a truncated sphere instead of an elongated ellipsoid as their aspect ratio of 0.62 might imply. All other bubbles, however, are still well approximated by a hemisphere and do not exhibit noticeable pinch off, as can also be seen in the second row of Fig. 2.

Classical bubbles were, on average, preceded by shorter waiting times and followed by longer waits until the next one. Nonclassical bubbles were preceded by longer waiting times and followed by shorter ones. This aspect of the data is analyzed in the Supplemental Material.

3. Radial displacement power

The consistent trends across the bubble modes presented in Figs. 3(a)–3(c), along with the apparent severity of bubble breakup, suggest that the spectrum in Fig. 2 might be organized according to the energy of these bubble growth modes. It is convenient to estimate a quantity we refer to as the radial displacement power,

$$P_{\mathrm{rd}} = \frac{E_{\mathrm{AK}} - E_{\mathrm{evap}}}{\Delta t}. \tag{1}$$

Here, Δt is the time for the bubble to grow to its maximum size. E_{AK} is the apparent kinetic energy, assuming a hemispherical bubble and an irrotational flow, estimated from the bubble wall motion defined as

$$E_{\mathrm{AK}} = \pi \rho_l \dot{R}^2 R^3, \tag{2}$$

where ρ_l is the liquid density, R is the equivalent bubble radius of an equivolume hemisphere, and $\dot{R}$ is the velocity of the liquid-vapor interface. An equivolume hemisphere is justified in the growth phase since the bubble remains nearly hemispherical in its early stages. Since the bubble also grows by evaporation, a simple measure of the bubble size evolution would lead to an overestimate of the kinetic energy, so we must subtract off the energy contribution from evaporation,

$$E_{\mathrm{evap}} = \rho_v|_{T_{\mathrm{sat}}, P_0}\, V_{\mathrm{evap}} \Delta h, \tag{3}$$

where ρ_v is the vapor density, V_{evap} is the bubble volume after the inertial expansion and collapse have decayed, indicated by the arrows in the plots of Fig. 2, and Δh is the enthalpy change accounting for changes in the latent and sensible heat. A more detailed description of these terms is derived in the Supplemental Material [49], with results plotted in Fig. 3(d). Since the radial displacement power increases with increasing bubble wall velocity, which in turn increases with the initial internal pressure of the bubble nucleus [52], P_{rd} provides us with an indirect measure of the energy available to the newly nucleated bubble. The radial displacement power follows the same trend as the other parameters: As the average size and apparent severity of breakup increases, so does the power.

4. Bubble stratification

It is interesting that for all bubbles beginning with the recoil bubble, their initial collapse creates a two-layer stratified system, as indicated in the third row of Fig. 2. It is known that bubble collapse can be accompanied by instabilities that grow due to geometrical effects such as breaks in the symmetry and perturbations of the initial bubble shape [41,53]. For bubbles located near a surface, geometrical constraints induce flow directed towards the surface as the bubble collapses, which is the origin of erosion in cavitation. The unorthodox-shaped bubbles in this experiment, however, wet the surface, and even

as they collapse, they appear to remain nearly pinned to the surface. As a result, the shape of collapsing bubbles resembles that of a bubble pinching off a gas nozzle [54–56], where the lower stratified layer serves the role of the nozzle, pinning the contact line, and the upper layer is the pinched-off bubble. As these bubbles experience both collapse and pinch off, the elongated neck typical of pinch-off experiments is shorter. When the collapse rate is relatively slow, such as for the recoil bubble, we observe the neck to be relatively symmetrical, typical of a gas bubble pinching off in water. When the collapse rate is relatively high, such as for implosion bubbles, the pinch off may become asymmetric, almost more akin to a droplet pinching off in air [54]. However, the low resolution of our high-speed images precludes detailed analysis.

C. Abundance of various bubble types

Bubbles with classical shape [14,22,57–59] were most abundant but bubbles with unorthodox shape were observed in at least half of our experiments. Figure 4 shows the relative abundance of bubbles of each type, displayed as histograms according to the heating power. The comparison is made according to two metrics: first simply according to the number of times each bubble was observed across all experiments, and secondly (to check for bias in the first analysis) according to the number of experiments containing this type of bubble. Each experiment consisted of a movie lasting 2 s, as described in the Experimental Section.

Just to observe bubbles is one thing; for cooling, it also matters how long bubbles interact with the surface. In this analysis, we compared relative times during which classical and nonclassical bubbles were observed. As summarized

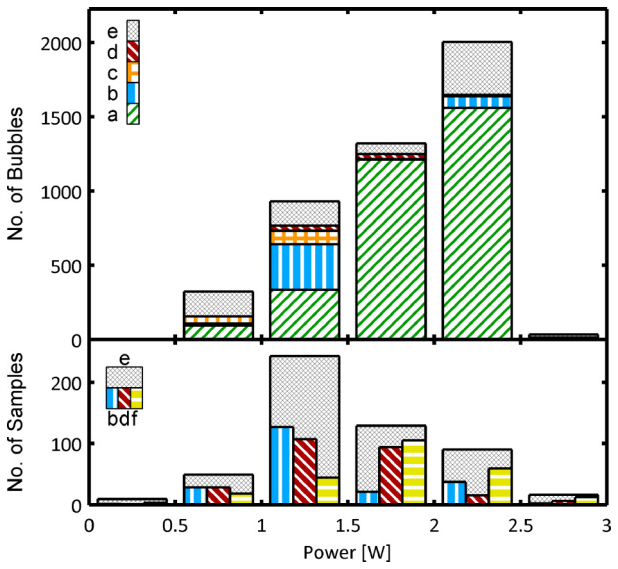

FIG. 4. (Color online) Relative abundance of bubbles of each type, displayed as histograms according to the heating power. The analysis is performed two ways: first simply according to the number of times each bubble was observed, secondly according to the number of experiments containing this type of bubble. (a) Green, classical; (b) blue, mushroom; (c) orange, explosions; (d) red, implosions; (e) black, other modes or simultaneous bubbles [49] (top) or total samples (bottom); and (f) yellow, persistent bubbles.

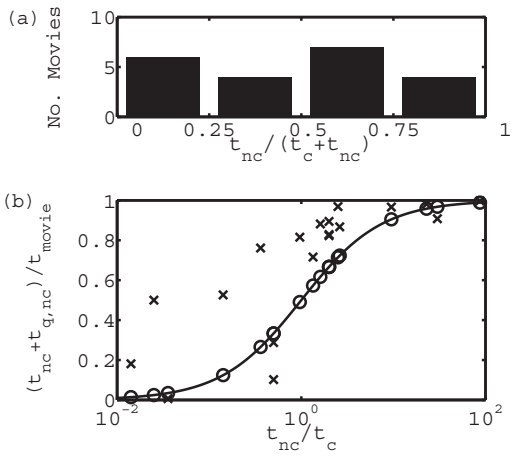

FIG. 5. Comparison of 21 experiments during which both classical and nonclassical bubble growth were observed. (a) Number of movies is tabulated according to the time fraction spent in nonclassical boiling modes. This data is grouped into quartiles as the nonclassical growth time (t_{nc}) normalized by total bubble growth time. (b) Including the effect of the associated quiescent time ($t_{q,nc}$), nonclassical bubbles contribute disproportionately more to the boiling time (×) than a ratio of the growth times might predict if the quiescent time were evenly apportioned between each mode (line, deg).

by the histograms in Fig. 5, 21 experiments that displayed both classical and nonclassical bubble growth were analyzed. In Fig. 5(a), relative, the fraction of time the bubble was nonclassical is compared to the total time that any bubble was observed, these data being compared across quartiles. The relatively flat distribution indicates that on average, when both classical and nonclassical modes are present, the system spends as much time growing classical bubbles as nonclassical bubbles, although any particular sample may show a bias towards one mode or the other. This suggests that when both modes are present, nonclassical bubbles should play a non-negligible role in the average heat transfer.

We find that when the heating power is relatively low, nonclassical bubbles are most dominant; in this regime they approach 50% of all the bubbles observed, but they were a minority when the heating power was highest. This presents an apparent paradox when considering that the nonclassical bubbles demonstrate a higher radial displacement power than classical bubbles. One can understand this apparent paradox by inspecting the relative timing of bubbles which occur at higher heating powers in samples containing both growth modes. While each movie had on average 23 bubbles, the bubbles were unevenly distributed in time such that several bubbles would succeed each other in short succession (<1 ms), followed by long quiescent periods (>10 ms). Such sequences typically contained 2–15 bubbles, although the average sequence contained four. These sequences typically consisted first of a large nonclassical bubble and then several smaller sequential classical bubbles which were each seeded by a residual bubble left attached to the surface by pinch off of the previous bubble, as is shown schematically in Fig. 6 and in the Supplemental Material [49]. The average lifetimes and probabilities of these bubbles are also plotted. On average, sequences were preceded

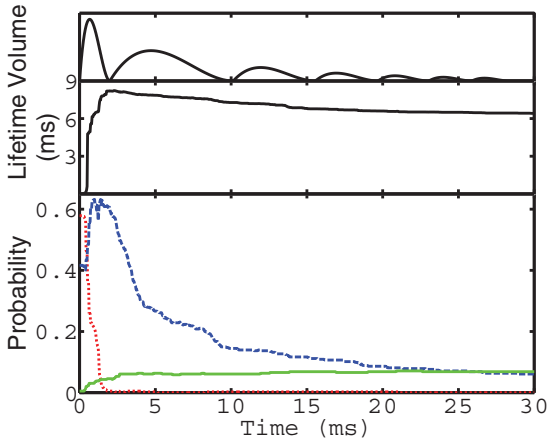

FIG. 6. (Color online) Dependence of the bubble properties on the time after the start of a sequence. Top: Schematic representation of bubble volumes in a sequence. The first bubble is generally a large, nonclassical bubble followed by a series of smaller classical bubbles. Middle: After the initial nonclassical bubble, the lifetime of subsequent bubbles diminishes as the sequence progresses. Bottom: The probability of a given bubble type as the sequence progresses: classical (dashed blue), persistent (solid green), and nonclassical (dotted red). After 25 ms, 80% of all sequences have terminated, although of the remaining sequences, half have entered a persistent state. Nonclassical bubbles appear at the beginning of the sequence and with a very low probability for the first 10 ms of the sequence.

by a quiescent time of 32 ms prior to the formation of a nonclassical bubble, and 60% of all sequences began with a nonclassical bubble, with mushrooms being the most common, comprising 43% of all initial nonclassical bubbles.

Following the initial, short-lived nonclassical bubble, a series of classical bubbles would be emitted, each with a shorter lifetime as plotted in Fig. 6. Occasionally a nonclassical bubble would form after the initial bubble, but they were rare with a probability of just 0.5%. Interestingly, each of these subsequent nonclassical bubbles were of the explosion class.

The relative abundance of classical bubbles appears to be influenced by flow patterns generated by the preceding nonclassical bubble. This mixing, which may be turbulent, tends to homogenize and lower the fluid temperature near the nucleation site, making the inertial overexpansion characteristic of nonclassical bubbles less likely, and encourages steady evaporation, and in this spirit we can understand the abundance of classical bubbles at high powers. At lower heating powers though, the cooling introduced by mixing following the departure of a nonclassical bubble may be sufficient to quench the growth of subsequent bubbles leading to fewer classical bubbles generated in the wake of mixing, driving up the relative proportion of nonclassical bubbles.

Clearly then, the quiescent time between bubble events also matters, because bubbles remove heat which has built up prior to the nucleation event and generate flow patterns which continue to cool the surface after departure events. It is therefore relevant to compare the incidence of nonclassical bubbles including the contributions of the quiescent time as shown in Fig. 5(b). Here, we compare the total time associated with the nonclassical bubbles, both due to growth ($t_{\rm nc}$) and during the quiescent time between bubbles ($t_{q,\rm nc}$), to the ratio between the growth times of the nonclassical and classical (t_c) bubbles. If the quiescent time contributed evenly to all modes, then the normalized nonclassical time would fall along the solid line, as is shown by the open circles. As described in the Supplemental Material [49], there are several reasonable methods to apportion the quiescent time to the surrounding bubbles. Here, we have chosen to do so by the relative size of the bubbles. Such an assumption is justified because larger bubbles should remove more heat built up prior to their arrival due to evaporation and generate larger flow patterns which take longer to decay than smaller bubbles. Using such an allotment, an average of 15% more time is associated with nonclassical bubbles than classical ones, indicated by the crosses. Since heat is being applied continuously, by comparing the associated time with each mode, we may therefore also estimate that nonclassical bubbles disproportionally remove more heat than classical ones. We should note that while the location of the crosses in Fig. 5 depends on the apportionment function that we select, the fact that the crosses lie above the curve for this allotment is tied to the physically meaningful characteristics of the nonclassical bubbles which are both larger and more widely spaced than their classical counterparts.

D. Persistent bubbles

After a period of boiling, in many experiments we observed the system to transition to a state in which a single, long-lived bubble remained pinned to the surface, inhibiting the formation of additional bubbles, and persisting until the heating laser was turned off and the experiment was stopped. Such persistent bubbles, with lifetimes greater than 100 ms, were observed at nearly every absorption power investigated (Fig. 4). Below 850 mW heating power, persistent bubbles grew slowly, starting just as soon as the laser was turned on. It seems that heat input to the bubble balanced conduction into the surrounding colder fluid, so bubbles did not grow large enough to overcome their surface pinning. Such trivial cases, which never developed into full-fledged boiling, were disregarded in the analysis of Fig. 4. At heating powers >850 mW, we measured the surface temperature to exceed 100 °C and buoyancy-driven liftoff was the rule, though some long-lived bubbles were still observed (20%). But at heating powers >1600 mW, 75% of all experiments displayed long-lived bubbles that could not be attributed to surface pinning, because their formation followed the earlier departure of other bubbles from the same surface position. For such bubbles to be stable despite the high heating power, they must reach a state where evaporation at the foot of the bubble is reduced so that it balances out condensation at the top of the bubble.

Beyond the single-bubble limit, the engineering literature has identified a related phenomenon known as the critical heat flux (CHF) of the boiling surface [6,60–62]. Below this point, when bubbles detach, the surface is rewet, quickly providing the potential to nucleate new bubbles. But above this point the surface is not rewet: The heated surface remains

coated with vapor, whose low thermal conductivity causes the surface temperature to escalate, often with destructive effects [52]. The growth of persistent bubbles, inhibiting the growth and departure of other bubbles, can be interpreted as the single-bubble equivalent of the CHF. It seems unusual that whereas nucleation-induced boiling was observed to begin at a heating power of 850 mW, these persistent bubbles that we interpret to reflect critical heat flux behavior were observed at a power twice this. This is probably because our system lacked the copious boiling that, by agitating the liquid, encourages bubbles to leave the surface in the more usual case of heating a surface uniformly.

More surprising is how this state was reached. While the traditional interpretation of the CHF refers to an inability of the surrounding liquid to rewet the surface, these experiments reveal that the process is more nuanced. Among the times that persistent bubble were observed, over 60% of the cases experienced a complete rewetting event immediately prior to the formation of the persistent bubble (Fig. SM8, Supplemental Material [49]). Following the rewetting event, bubbles grew slowly, gradually pushing the contact line to wider diameters while remaining pinned to the surface, eventually stabilizing as the evaporation near the contact line balanced the condensation at the top of the bubble. The observed rewetting suggests a new CHF mechanism that may have a useful engineering implication: If the pinning force at the contact line is sufficiently strong to allow a bubble to fully cover a microheater, then the surface may experience a gradual dryout.

As a rule of thumb, bubbles lasting longer than 100 ms did not depart on their own, and the overwhelming majority of them persisted to the end of the experiment. In occasional experiments, though, we observed bubbles to be removed from the surface through the nucleation of a second bubble within the heated surface area. In such cases, the preexisting, long-lived bubble would be removed when a second bubble suddenly nucleated and grew, thus kicking off the first bubble, or when the second bubble merged with the original bubble leading to the departure of both bubbles (Fig. SM9, Supplemental Material [49]). Through the interplay between bubbles, persistent bubbles could be removed, thereby providing a mechanism to raise the critical heat flux of a given surface.

IV. CONCLUSIONS

Through empirical analysis of high-speed optical microscopy data, we have categorized the diversity of behavior seen when bubbles boil into cooler water. While bubbles with classically symmetric shape are most prevalent, bubbles of nonclassical shape appear to contribute more to the overall heat transfer when they are present. The morphologies of such bubbles appear to be induced by the complete dewetting of the liquid phase under the bubble, and pinning of the bubble edges as it collapses. No relation was observed between bubble size and heating power, but a preference for classical bubbles was seen at higher powers. The reason for this preference is unclear, but it may be that the continuous mixing induced by the departure of many smaller bubbles increases the likelihood of further such bubbles, acting as a positive feedback loop. In addition, these experiments also captured some rare events that help to understand bubble-bubble interactions. While localized heating had the advantage of nicely defining the experimental system, it limited the experimental boiling window to the narrow heating power range between 850 and 1600 mW. Above and below this range, bubbles remained pinned to the surface.

Bubbles often followed one another in complex sequences. Violent explosion, a common departure mechanism, was often followed up by slower-growing classical bubbles. The violence of the first bubble in the sequence likely served two important functions. First, it likely homogenized temperature in the liquid nearby, enabling the slower-growing bubbles to take hold. Second, as exploding bubbles broke up, they provided additional nucleation sites which grew when sufficiently close to the heating area. Extrapolating this to the everyday case of boiling where a surface is uniformly heated such that numerous bubbles are present simultaneously, we infer that the turbulence generated by some explosive departures may enhance the likelihood of slow and controlled growth of later classically shaped bubbles.

ACKNOWLEDGMENTS

We thank Dr. Sung Chul Bae for help in designing the instrument. This work was supported by the Office of Naval Research MURI program, Grant No. N00014-07-1-0723.

[1] J. Mitrovic, Int. J. Therm. Sci. **45**, 1 (2006).
[2] S. Siedel, S. Cioulachtjian, and J. Bonjour, Exp. Therm. Fluid Sci. **32**, 1504 (2008).
[3] C. Gerardi, J. Buongiorno, L. Hu, and T. McKrell, Int. J. Heat Mass Transf. **53**, 4185 (2010).
[4] S. K. Roy Chowdhury and R. H. S. Winterton, Int. J. Heat Mass Transf. **28**, 1881 (1985).
[5] S. G. Kandlikar and M. E. Steinke, Int. J. Heat Mass Transf. **45**, 3771 (2002).
[6] R. Chen, M.-C. Lu, V. Srinivasan, Z. Wang, H. H. Cho, and A. Majumdar, Nano Lett. **9**, 548 (2009).
[7] T. Lüttich, W. Marquardt, M. Buchholz, and H. Auracher, Int. J. Therm. Sci. **45**, 284 (2006).
[8] Y. Qiu and Z. Liu, Int. J. Heat Mass Transf. **51**, 1683 (2008).
[9] K. T. Hong, H. Imadojemu, and R. L. Webb, Exp. Therm. Fluid Sci. **8**, 279 (1994).
[10] L. Liao, R. Bao, and Z. Liu, Heat Mass Transfer **44**, 1447 (2008).
[11] Z. Guo and M. S. El-Genk, Int. J. Heat Mass Transf. **35**, 2109 (1992).
[12] H. Zhang, I. Mudawar, and M. M. Hasan, Int. J. Heat Mass Transf. **45**, 4079 (2002).
[13] G. Sateesh, S. K. Das, and A. R. Balakrishnan, Int. J. Heat Mass Transf. **48**, 1543 (2005).
[14] M. G. Cooper and A. J. P. Lloyd, Int. J. Heat Mass Transf. **12**, 895 (1969).
[15] A. Mukherjee and S. G. Kandlikar, Int. J. Heat Mass Transf. **50**, 127 (2007).
[16] D. Li and V. K. Dhir, J. Heat Transf. **129**, 864 (2007).

[17] H. K. Forster and N. Zuber, AIChE J. **1**, 531 (1955).
[18] A. Sakurai, M. Shiotsu, K. Hata, and K. Fukuda, Nucl. Eng. Des. **200**, 39 (2000).
[19] N. Basu, G. R. Warrier, and V. K. Dhir, J. Heat Transf. **124**, 717 (2002).
[20] H. Auracher and W. Marquardt, Int. J. Heat Fluid Flow **25**, 223 (2004).
[21] C.-J. Kuo and Y. Peles, Int. J. Heat Mass Transf. **50**, 4513 (2007).
[22] J. Kim, Int. J. Multiphase Flow **35**, 1067 (2009).
[23] K. M. Balss, C. T. Avedisian, R. E. Cavicchi, and M. J. Tarlov, Langmuir **21**, 10459 (2005).
[24] C. T. Avedisian, W. S. Osborne, F. D. McLeod, and C. M. Curley, Proc. R. Soc. London, Ser. A **455**, 3875 (1999).
[25] C. T. Avedisian, R. E. Cavicchi, and M. J. Tarlov, Rev. Sci. Instrum. **77**, 063706 (2006).
[26] J. G. Myers, V. K. Yerramilli, S. W. Hussey, G. F. Yee, and J. Kim, Int. J. Heat Mass Transf. **48**, 2429 (2005).
[27] S. Moghaddam and K. Kiger, Int. J. Heat Mass Transf. **52**, 1284 (2009).
[28] O. C. Thomas, R. E. Cavicchi, and M. J. Tarlov, Langmuir **19**, 6168 (2003).
[29] A. G. G. Toh, M. G. Nolan, R. Cai, and D. L. Butler, Proc. SPIE **6800**, 680004 (2007).
[30] M. Miyauchi, N. Kieda, S. Hishita, T. Mitsuhashi, A. Nakajima, T. Watanabe, and K. Hashimoto, Surf. Sci. **511**, 401 (2002).
[31] M. Miyauchi, A. Nakajima, T. Watanabe, and K. Hashimoto, Chem. Mater. **14**, 2812 (2002).
[32] R.-D. Sun, A. Nakajima, A. Fujishima, T. Watanabe, and K. Hashimoto, J. Phys. Chem. B **105**, 1984 (2001).
[33] N. Sakai, R. Wang, A. Fujishima, T. Watanabe, and K. Hashimoto, Langmuir **14**, 5918 (1998).
[34] T. Bonometti and J. Magnaudet, Phys. Fluids **18**, 052102 (2006).
[35] M. S. Plesset and A. Prosperetti, Annu. Rev. Fluid Mech. **9**, 145 (1977).
[36] Lord Rayleigh, Philos. Mag. Ser. 6 **34**, 94 (1917).
[37] A. Vogel, N. Linz, S. Freidank, and G. Paltauf, Phys. Rev. Lett. **100**, 038102 (2008).
[38] J. R. Blake and D. C. Gibson, J. Fluid Mech. **111**, 123 (1981).
[39] T. B. Benjamin and A. T. Ellis, Philos. Trans. R. Soc. London, Ser. A **260**, 221 (1966).
[40] O. Lindau and W. Lauterborn, J. Fluid Mech. **479**, 327 (2003).
[41] J. R. Blake, B. B. Taib, and G. Doherty, J. Fluid Mech. **170**, 479 (1986).
[42] E. Klaseboer, K. C. Hung, C. Wang, C. W. Wang, B. C. Khoo, P. Boyce, S. Debono, and H. Charlier, J. Fluid Mech. **537**, 387 (2005).
[43] M. S. Plesset and R. B. Chapman, J. Fluid Mech. **47**, 283 (1971).
[44] J. R. Blake and D. C. Gibson, Annu. Rev. Fluid Mech. **19**, 99 (1987).
[45] J. P. Padilla-Martinez, G. Aguilar, J. C. Ramirez-San-Juan, and R. Ramos-García, Proc. SPIE **8097**, 809727 (2011).
[46] X. Noblin, A. Buguin, and F. Brochard-Wyart, Eur. Phys. J. E **14**, 395 (2004).
[47] M. Ramiasa, J. Ralston, R. Fetzer, R. Sedev, D. M. Fopp-Spori, C. Morhard, C. Pacholski, and J. P. Spatz, J. Am. Chem. Soc. **135**, 7159 (2013).
[48] I. S. Fayzrakhmanova, A. V. Straube, and S. Shklyaev, Phys. Fluids **23**, 102105 (2011).
[49] See Supplemental Material at http://link.aps.org/supplemental/10.1103/PhysRevE.89.013011 for further analysis, figures, and a movie depicting the various growth modes.
[50] S. Parker, Ph.D. thesis, University of Illinois at Urbana-Champaign, 2014.
[51] J.-P. Franc and J.-M. Michel, *Fundamentals of Cavitation* (Kluwer Academic Publishers, Dordrecht, 2004).
[52] V. P. Carey, *Liquid Vapor Phase Change Phenomena: An Introduction to the Thermophysics of Vaporization and Condensation Processes in Heat Transfer Equipment*, 2nd ed. (Taylor & Francis, London, 2007).
[53] O. R. Enriquez, I. R. Peters, S. Gekle, L. E. Schmidt, D. Lohse, and D. van der Meer, J. Fluid Mech. **701**, 40 (2012).
[54] J. C. Burton, R. Waldrep, and P. Taborek, Phys. Rev. Lett. **94**, 184502 (2005).
[55] N. C. Keim, P. Møller, W. W. Zhang, and S. R. Nagel, Phys. Rev. Lett. **97**, 144503 (2006).
[56] S. T. Thoroddsen, T. G. Etoh, and K. Takehara, Phys. Fluids **19**, 042101 (2007).
[57] T. Fuchs, J. Kern, and P. Stephan, J. Heat Transf. **128**, 1257 (2006).
[58] R. C. Lee and J. E. Nydahl, J. Heat Transf. **111**, 474 (1989).
[59] G. Son and V. K. Dhir, Int. J. Heat Mass Transf. **51**, 2566 (2008).
[60] S. J. Ha and H. C. No, Int. J. Heat Mass Transf. **41**, 3771 (1998).
[61] V. S. Nikolayev and D. A. Beysens, Europhys. Lett. **47**, 345 (1999).
[62] S. G. Kandlikar, J. Heat Transf. **123**, 1071 (2001).